Haruna et al. Beni-Suef University Journal of Basic and Applied Sciences (2020) 9:8
https://doi.org/10.1186/s43088-020-0033-9

Beni-Suef University Journal of Basic and Applied Sciences

RESEARCH Open Access

Effect of annealing temperature on the synthesis and photocatalytic properties of $Bi_{0.65}K_{0.2}Ba_{0.15}FeO_3$ perovskite-like nanoparticle synthesized by sol-gel method

Abdurrashid Haruna*, Ibrahim Abdulkadir and Sulaiman Ola Idris

Abstract

Background: $BiFeO_3$ shows promising applications in photocatalytic degradation, purification process, and in clean energy generation. The various fascinating properties of bismuth ferrite nanoparticles can be improved by doping the material at either of the A or B sites to give it extra photocatalytic advantage toward decreasing the energy bandgap and other photophysical properties of the material.

Results: In this research, pure $Bi_{0.65}K_{0.2}Ba_{0.15}FeO_3$ perovskite material was synthesized using the sol-gel method via citric acid route in the presence of sodium dodecyl sulfate (SDS). The powdered nanoparticles were annealed at different annealing temperatures of 600, 700, and 800 °C each for 4 h in a muffle furnace and coded K2BFO 600, K2BFO 700, and K2BFO 800 corresponding to the annealing temperature of each portion. The powder nanoparticles were characterized using powdered X-ray diffraction (PXRD) to determine the crystallite structure. The samples displayed similar peak patterns with increase in intensity as the annealing temperature is increased indicating an increase in crystallinity. The impurity peaks in K2BFO 800, however, show that the sample may contain a secondary phase. Scanning electron microscopy (SEM) was used to determine the morphology, and UV-Vis spectroscopy indicated that all the powders were photoactive within the visible region of the electromagnetic spectrum. ATR-FTIR spectra of the samples were collected to study the formation and phase purity of the B-site in the perovskite structures. The photocatalytic performance of the powder was tested on methylene blue dye under visible light irradiation for the degradation studies. All powders showed photocatalytic ability after 2 h of irradiation with the powder annealed at 800 °C being better. The photocatalytic activities of the powders showed improvement on addition of 2 drops of 1 M H_2O_2 (80% degradation for K2BFO 800). The bandgap energy of K2BFO 800, 700, and 600 was estimated at approximately 2.00, 2.12, and 2.18 eV, respectively, using Tauc's equation. The improved activity is as a result of photoabsorption of visible light by the doped powders causing generation of electrons and holes. The kinetic studies were carried out and the mechanisms of the photocatalytic reaction proposed.

Conclusion: The effect of annealing temperature on synthesis of the material shows enhanced photoactivity in the presence of hydrogen peroxide leading to improved performance for the degradation of MB, and the catalyst can be said to be a good candidate for the treatment of waste materials.

Keywords: Sol-gel method, Doping effects, Methylene blue, Nanoparticle, Photocatalyst

* Correspondence: abdurrashid.haruna@yahoo.com
Department of Chemistry, Ahmadu Bello University, Zaria, Nigeria

1 Background

Over the last few years, the increasing use of noble metals to improve the photocatalytic performance of materials is an area of interest for most researchers. $BiFeO_3$ (BFO) nanoparticle doped with metal cations has shown great promise in enhancing the photocatalytic performance of materials finding numerous applications. Doping of BFO with univalent, trivalent, and other noble metal ions has been a way of enhancing the photocatalytic properties of semiconducting materials. This promising area is drawing attention in wastewater treatment, environmental remediation, air purification, industrial waste processes, and in the destruction of other toxic chemicals [1–8].

Active photocatalyst in the presence of sunlight converts waste substances, pollutants, and other contaminants to harmless products, carbon dioxide, and water. To date, energy generation and environmental cleaning processes are finding potential applications useful in numerous photo-chemical reactions [9]. A photoreaction is an important chemical reaction induced by photoabsorption of a solid material that remains unchanged during a reaction [10]. Photocatalyst has long been studied for environmental applications and in clean energy generation. A large number of photocatalytic reactions, however, have increased sharply over the past 2 decades and a variety of new materials have been significantly developed [11]. In particular, the photocatalytic hydrogen production from water-splitting has been of very significant interest using the solar energy [12].

Perovskites are class of inorganic compounds with the general formula of ABO_3 [13]. In its cubic structure, the A-site cation is occupied by a large metal while the B-site is occupied by a small element such as that of transition element [14]. The perovskites exhibit various properties suitable for numerous technological applications [15]. The multiferroic behavior of BFO and BFO-related material as well as the excellent photocatalytic properties when doped with Sr^{2+} was reported [16–18]. Studies have shown that the photoactivity of catalysts is influenced by a wide variety of factors such as the method of catalysts preparation, the adsorption affinity and capacity for organic contaminants, the crystal morphology, and the size [19]. Much work has been reported on the different synthesis methods of BFO, but there is still the need to study the effect of doping the material and to investigate the impact on its crystal structure [20]. Hu et al. reported the photocatalytic property of Sm-doped BFO nanoparticle for the degradation of methyl orange under visible light which showed a reduce energy bandgap of 2.06 eV [21].

Doping is used to modify the structure of an existing catalyst giving it an extra photocatalytic advantage. The properties of a perovskite material can be influenced by doping with smaller ions to improve on the existing material [22]. The introduction of a suitable dopants as impurity lowers the bandgap energy of a semiconducting material. It increases the number of electrons in the conduction band and eventually slows down the recombination process, hence serving a better photocatalytic activity. The studies were carried out to evaluate the effect of doping, and some relevant parameters like the effect of annealing temperature and the addition of hydrogen peroxide and the photocatalytic degradation of MB dye pollutants. In this research, $Bi_{0.65}K_{0.2}Ba_{0.15}FeO_3$ nanoparticle was synthesized by the sol-gel process. SDS was used in the synthesis procedure to ensure the nucleation of the particles and the limited growth of the crystals. The structure of the synthesized nanoparticle as annealing temperature increases was investigated, and also, the photocatalytic properties of the material under UV-visible irradiation were determined. The kinetic studies were carried out and the mechanisms of the photocatalytic reaction proposed.

2 Methods

2.1 Materials

Barium nitrate $(Ba(NO_3)_2)$, $Fe(NO_3)_3{\cdot}9H_2O$, $Bi(NO_3)_3.5H_2O$, KNO_3, $C_6H_8O_7{\cdot}H_2O$, sodium dodecyl sulfate (SDS), HCl, NaOH, NH_4OH, H_2O_2, and ethylene glycol. Distilled water was used throughout the experiment. All chemicals used in this research were of analytical grade purchased from the Sigma-Aldrich Chemical Company and used without further purification.

2.2 Synthesis of $Bi_{0.65}K_{0.2}Ba_{0.15}FeO_3$

Potassium-doped bismuth barium ferrite $Bi_{0.65}K_{0.2}Ba_{0.15}FeO_3$ powders were prepared by the sol-gel method in the presence of sodium dodecyl sulfate via citric acid route. Calculated amounts of analytical grade chemicals $Ba(NO_3)_2$, $Fe(NO_3)_3{\cdot}9H_2O$, $Bi(NO_3)_3.5H_2O$, and of KNO_3 precursors were dissolved in 100 ml of distilled water. Citric acid was added (molar ratio to nitrate salts 21) with continuous stirring at 90 °C for about 50 min. Ethylene glycol was added to the mixture under continuous heating and stirring at 90 °C for 1 h. SDS was added to the solution and then a few drops of ammonium hydroxide (30% NH_3) was added to the mixture solution to maintain a pH = 8. A gel was formed and the gel obtained was removed from the beaker and placed to dry in an oven at 120 °C for 6 h to obtain a dry porous solid which was then crushed to give the as-prepared powder. The powder was thereafter split into three portions and then annealed at various annealing temperatures ranging from 600–800 °C in a muffle furnace for 4 h each at 1 °C/min. The samples were coded K2BFO 600, K2BFO 700, and K2BFO 800.

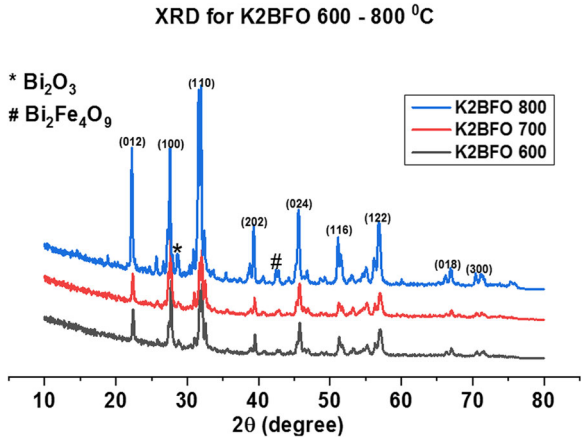

Fig. 1 Powder X-ray diffraction peaks for $Bi_{0.75}K_{0.2}Ba_{0.15}FeO_3$ annealed at temperature 600–800° C

2.3 Characterization

The crystallite structure was studied using the powder X-ray diffraction (PXRD) pattern measured on a Rigaku Ultima IV X-ray diffractometer using the Cu Kα (λ = 1.5406 Å). The morphology of the sample was studied by scanning electron microscopy (SEM) using the JEOL/EO Version 1.0 (JSM-6610). The scanning was performed between 10 and 80° 2θ with a scanning speed of 3°/min at 40 kV and 40 mA. UV-vis spectrophotometer (Agilent Technology, Cary Series) was used throughout in taking the absorbance measurement. The ATR–FTIR of the nanopowders was performed at room temperature using the PerkinElmer spectrum 100 Fourier transform infrared (FTIR).

2.4 Photocatalytic activity

The photocatalytic activity of the powder was tested on methylene blue (MB) dye solution under visible light irradiation for 2 h. A 10-mg/L solution of MB dye was prepared and used with the catalyst loading of 15 mg for the degradation experiment. The photodegradation studies of MB were evaluated in a fabricated continuous stir tank photoreactor with a magnetic stirrer at 50 rpm and 250 W visible lamp (Osram, Germany) placed 7 cm above the beaker. The concentration of MB dye was determined at approximately the wavelength of maximum absorption (λ_{max} = 664 nm) using the UV–vis spectrophotometer. In the absence of visible light, a 100 ml of 10 mg/L MB dye solution was adjusted at natural pH 7 with NaOH and HCl was continuously stirred using a magnetic stirrer for 2 h at 20 min interval for all samples. Ten milliliters of the solution was taken after every 20 min for absorbance measurement. This procedure was repeated under visible lights with the catalyst for the same periods until all data were gathered. In each case, the 10 ml was taken for absorbance measurement. The effects of the addition of 1 M H_2O_2 (peroxide) was investigated.

Table 1 Lattice parameters and the crystallite sizes for the $Bi_{0.65}K_{0.2}Ba_{0.15}FeO_3$ annealed at temperatures of 600, 700, and 800° C

Samples	Space group	Cell parameters			Crystallite size (nm)
		a (Å)	b (Å)	c (Å)	
K2BFO 600	*R3C*	5.496	5.496	13.327	20.32 ± 2
K2BFO 700	*R3C*	5.482	5.482	13.312	24.16 ± 2
K2BFO 800	*R3C*	5.491	5.491	13.232	27.12 ± 2

3 Results

3.1 Formation of perovskite nanoparticle

Perovskite nanoparticles were synthesized using the sol-gel method in the presence of sodium dodecyl sulfate. The prepared powder was annealed at different annealing temperatures of 600, 700, and 800° C each for 4 h. The material was applied as a photocatalyst against MB dye pollutant, and the wavelength of maximum absorption of MB dye solution scanned between 200 and 800 nm was approximately determined and found to be at 664 nm.

3.2 X-ray diffraction of $Bi_{0.75}K_{0.2}Ba_{0.15}FeO_3$ particles

The X-ray diffraction pattern of the samples prepared under different conditions was measured on a Rigaku Ultima IV X-ray diffractometer. The powdered X-ray diffraction patterns of the powders annealed at temperatures of 600, 700, and 800° C are shown in Fig. 1. The lattice parameters and the average crystallite sizes of powders as estimated from the Debye Scherer equation are shown in Table 1.

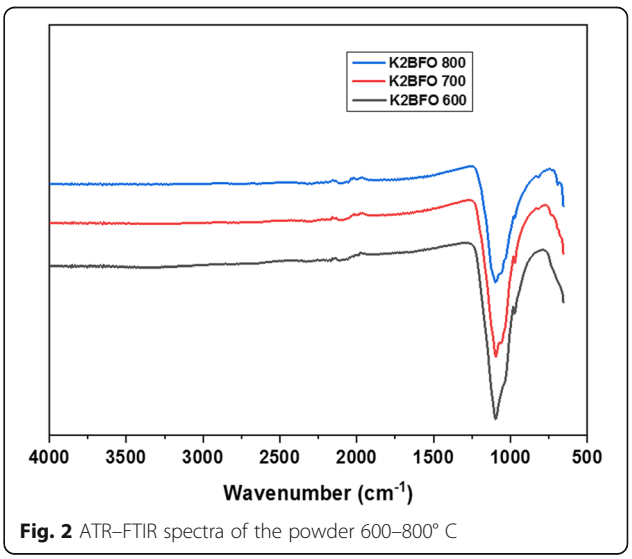

Fig. 2 ATR–FTIR spectra of the powder 600–800° C

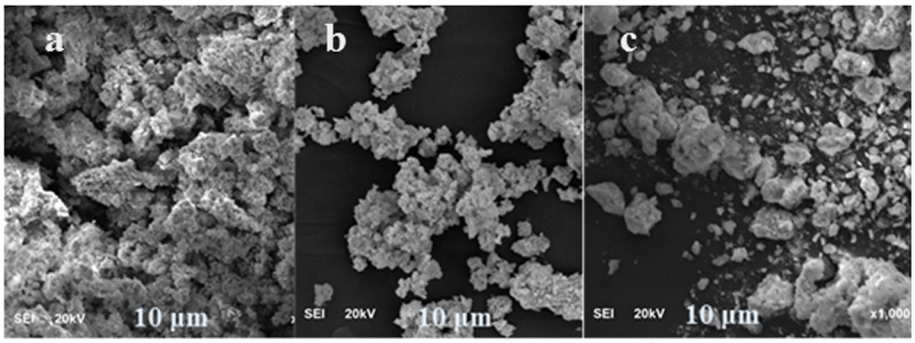

Fig. 3 SEM images of $Bi_{0.65}K_{0.2}Ba_{0.15}FeO_3$ nanoparticle synthesized at temperatures between 600 and 800° C

3.3 ATR–FTIR spectra of $Bi_{0.75}$ $K_{0.2}Ba_{0.15}FeO_3$ nanoparticle

The ATR–FTIR spectra of the samples were measured at room temperature as shown in Fig. 2 and are collected at 500–4000 cm^{-1} using the attenuated total reflectance Fourier transform infrared.

3.4 SEM image of the particles

The SEM images of the perovskite nanoparticles annealed at different temperatures are shown in Fig. 3 for the morphological analysis.

3.5 Photocatalytic activities of $Bi_{0.65}K_{0.2}Ba_{0.15}FeO_3$

The photodegradation of MB was tested on separate samples of the powdered catalyst under visible light irradiation in the presence and absence of hydrogen peroxide as presented in Fig. 4. The variation of degradation rate (C/C_o) versus irradiation time at 20 min interval for 2 h was carried out for MB photodegradation using the perovskite nanoparticles at different annealing temperatures of 600, 700, and 800 °C.

Table 2 shows the degradation efficiencies, and the effect of hydrogen peroxide of the nanoparticles at various temperatures, in each case powder annealed at a higher temperature, indicate higher degradation efficiencies probably due to the concentration of dopants. Comparison of the rate of degradation of organic pollutants for pure BFO and BFO-doped nanoparticles using different light sources and time interval are shown in Table 3

3.6 Uv-vis DRS spectroscopy of the nanoparticle

The Uv-visible DRS spectroscopy of the powdered samples is shown in Fig. 5. The optical absorption of the samples shows a strong photo-absorption property in the visible light region (400–600 nm) of the electromagnetic spectrum.

3.7 Kinetic studies and mechanism of degradation

Figure 6 shows the kinetic studies of $Bi_{0.65}K_{0.2}Ba_{0.15}FeO_3$ (600–800 °C) nanoparticles. The observed rate constants for the degradation of MB dye with the catalyst are presented in Table 4.

4 Discussions

4.1 Characterization of all samples

The PXRD pattern is presented in Fig. 1 and shows the Bragg peaks with Miller indices associated with the rhombohedral structure of BFO, and they are in good agreement with the JCPDS file for BFO (JCPDS card No. 86-1518). The powder annealed at 600 °C shows the beginning of the formation of crystal, nucleation stage. At higher temperatures of 700 and 800 °C however, the growth of prominent peaks showed that all the ions are

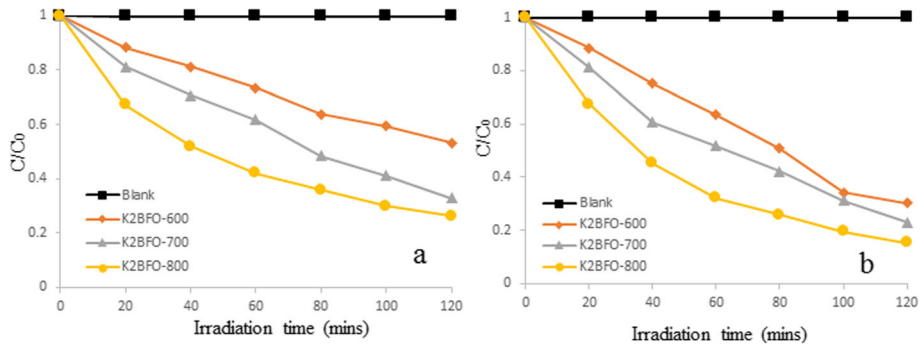

Fig. 4 MB photodegradation of K2BFO 600–800° C (a) in the absence of peroxide (b) in peroxide

Table 2 Degradation efficiency (%) of K2BFO on MB in the presence and absence of peroxide

S/N	Catalyst	Effect of peroxide	Time (h)	% Degradation $\frac{C_o - C_t}{C_o} \times 100$
1	K2BFO–600	–	2	57
2	K2BFO–700	–	2	67
3	K2BFO–800	–	2	74
4	K2BFO–600	1 M H_2O_2	2	66
5	K2BFO–700	1 M H_2O_2	2	73
6	K2BFO–800	1 M H_2O_2	2	80

properly incorporated into the perovskite structure with the presence of minor impurity peaks at all temperatures [30]. These impurity peaks become more prominent for K2BFO 800, indicating that the sample, at this temperature may contain a secondary phase. Maximum intensity peaks at higher temperatures indicate a high crystallinity of the powder. This is because high crystallinity is accompanied by prominent peaks as a result of increasing annealing temperatures. The peak at around 28° and 44° are assigned to Bi_2O_3 and $Bi_2Fe_4O_9$, respectively, occurring as secondary phases at all calcination temperatures. This is due to the partial reaction or loss of Bi because of its volatility as similarly reported from previously [31–33]. Also, BFO nanoparticles have been synthesized by various researchers using different methods from the review of literature showing similarity in the diffraction peaks of K2BFO particles [23, 24, 34]. The average crystallite size of the materials is shown in Table 1 and was determined by using the Debye-Scherrer equation. There is an observed change in the average crystallite size of the powders and with the most prominent peak (110). All the peak reflection with lattice parameters $a = b = 5.491$ Å and $c = 13.232$ Å were easily indexed to the pure rhombohedral structure of BFO as previously reported [23].

The ATR–FTIR spectra of the powders K2BFO 600–800 were collected at room temperature and are shown in Fig. 2. The broadband peak at 850–1350 cm^{-1} is assigned to the powdered nanoparticles for all the samples indicating B-site formation of the perovskite structure as a result of adsorbed water molecule onto the surface of the material. A stretching and bending vibrations at lower wavenumbers of the perovskite nanomaterial may as well suggest the formation of O–Fe–O, metal-oxygen bonds, and Fe–O in the perovskite structure similar to that previously reported [30].

The morphology of the crystals viewed on the surface of the materials is shown in Fig. 3. The structural changes of the particles leading to the formation of the crystalline phase are a result of the increase in calcination temperature. It can be seen from Fig. 3a, the nucleation and the formation of polycrystalline nanoparticles indicating that perovskite nanoparticles are formed at an annealing temperature of 600° C. As the calcination temperature increases (Fig. 3b, c), there is the agglomeration of the particles in different sizes which are seen to be clearly uniform, although there is a significant change in the size and shape of the primary particles attributing it to the effect of increasing annealing temperature for the particles at 800° C. The SEM image results are in agreement with the presented XRD result.

4.2 Photocatalytic activity of all samples

The photocatalytic activity of the powdered nanoparticles was tested at room temperature on MB dye and is evaluated under the visible light irradiation for 2 h. Figure 4 shows the degradation curve of all powders in the absence and presence of hydrogen peroxide. The photodegradation of the dye with a few drops of H_2O_2 only shows little degradation. All powders showed

Table 3 Comparison of the rate of degradation of organic pollutants for pure BFO and BFO-doped nanoparticles using different light sources and time interval

Study	Dopants	Organic pollutant	Source of light	Concentration of dye (mg/L)	Time (h)	Degradation efficiency (%)	Reference
K2BFO	Ba, K	Methylene blue	Visible light	10.00	2.00	80	This study
BFO	Sr	Methyl orange	Visible light	20.00	2.00	95	[23]
BFO	Ba	Benzene	Visible light	10.00	1.00	97	[24]
BFO	Ba, Na	Methylene blue	Visible light	10.00	1.50	84	[25]
TiO_2	Pt	Methyl orange	UV light	20.00	1.50	98	[26]
TiO_2	Ce	Rhodamine B	UV light	0.50	2.00	80	[27]
TiO_2	S	4-Chlorophenol	Visible light	0.32	6.00	88	[28]
BFO	Ba	Methyl orange	Visible light	10.00	2.00	81	[29]

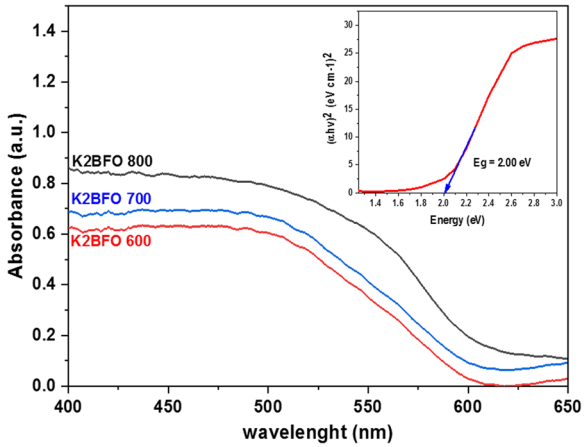

Fig. 5 UV-vis DRS spectrum of $Bi_{0.65}K_{0.2}Ba_{0.15}FeO_3$ nanoparticle synthesized by sol-gel method

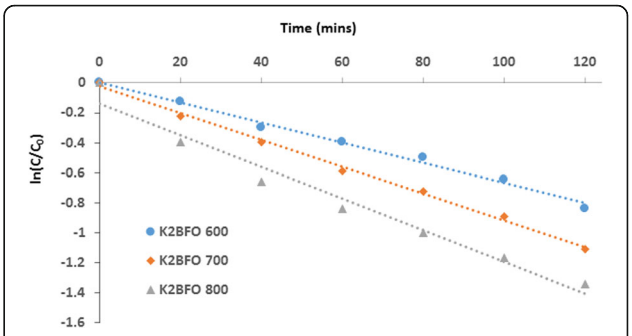

Fig. 6 First-order kinetics of MB photodegradation

photocatalytic ability after 2 h of irradiation with the powder annealed at 800° C being the best. The photocatalytic activities of the powders showed improvement on the addition of 2 drops of 1 M H_2O_2 (80% degradation for K2BFO 800). Table 2 shows the actual percentage efficiencies of all powders in the presence and absence of hydrogen peroxide. The improved photoactivity is due to the activation of peroxide by the nanoparticles to generate more reactive hydroxyl radicals [35]. The photodegradation studies of BFO with MB show that MB could effectively be degraded under the visible-light irradiation [31]. The degradation of BFO doped with Ba^{2+} has shown an enhanced activity of 97 % for benzene removal after 1 h of visible light irradiation [24].

The UV-visible DRS spectrum of the powders is shown in Fig. 5. The materials absorbed light strongly within the visible region (400–800 nm) of the electromagnetic spectrum, and the optical absorption of the samples showed a strong photoabsorption property. The corresponding bandgap energies for all the materials were calculated from the linear portion of a Tauc's plot of $(\alpha h\nu)^2$ against $h\nu$ using the Tauc's equation [36], where $h\nu$ is the photo energy and α is the absorption coefficient. The energy bandgap values for K2BFO 800, K2BFO 700, and K2BFO 600 were estimated at 2.00, 2.12, and 2.18 eV, respectively. The obtained values are compared with the results of previous studies where the energy values of 2.10 and 2.15 eV were determined [37]. Thus, from the presented energy result, $Bi_{0.65}K_{0.2}Ba_{0.15}FeO_3$ nanoparticle may have a promising application as a visible-light-driven photocatalyst in the treatment of wastewater.

The rate constants for MB degradation based on the first-order kinetics was determined quantitatively by using the equation $\ln(C/C_o) = k_{obs}t$) [38], where k_{obs} is the observed rate constant, C_o and C are the initial and final concentrations at time t (min), respectively, for the dye as shown in Fig. 6. The catalyst as annealing temperature increases leads to an increase in the rate constants for the pseudo-first-order kinetics. This is clearly shown in Table 4. The rate constants of the powdered materials increase with increasing annealing temperatures due to the doping of the ion into the structure leading to enhance photoactivity of the powders. For the purpose of comparison, however, the percentage photodegradation (%) of different organic dye pollutants at different time intervals were reported previously for doped and undoped BFO nanomaterials with other catalysts as shown in Table 3.

A mechanism of MB photodegradation with the catalyst is proposed for the entire photodegradation process. The following Eqs. 1–4 show the photocatalytic process involving the photogeneration of electron-hole pairs. In the mechanistic pathway, therefore, the electron generated in the conduction band of the catalyst is trapped by peroxide causing the production of highly reactive hydroxyl radicals. The radicals generated are responsible for the degradation of methylene blue organic dye.

$$\mathrm{K2BFO} + h\nu \rightarrow \mathrm{h}^+ + e^- \quad (1)$$

$$\mathrm{H_2O_2} + e^- \rightarrow \mathrm{OH^\bullet} + \mathrm{OH^-} \quad (2)$$

$$\mathrm{H_2O} + \mathrm{h}^+ \rightarrow \mathrm{OH^\bullet} + \mathrm{H}^+ \quad (3)$$

$$\mathrm{OH^\bullet} + \mathrm{MB} \rightarrow \text{degradation of dye} \quad (4)$$

Table 4 Observed rate constant for the photodegradation of model MB dye in 15 mg of the photocatalyst

System	R^2	K_{obs}/min^{-1}
K2BFO 600	0.9913	6.65×10^{-3}
K2BFO 700	0.9966	8.81×10^{-3}
K2BFO 800	0.9680	1.10×10^{-2}

5 Conclusion

In conclusion, a *K*-doped perovskite-like $Bi_{0.65}K_{0.2}Ba_{0.15}FeO_3$ nanoparticle was synthesized using the sol-gel method in the presence of SDS and ethylene glycol via the citric acid route. The PXRD peaks show that the powders crystallized in a rhombohedral structure with *R3C* space group. K2BFO 600 and 700 were single phases while K2BFO 800 showed peaks indicative of the presence of a secondary phase. SEM micrographs of all samples show uniformity in the particle size and morphology of the crystallites at each annealing temperature, in agreement with the presented PXRD results. The photocatalytic performance of the perovskite nanoparticle powders record good activity for the degradation of MB dye. The bandgap energy values obtained may suggest that the material may have some promising applications as a photoactive substance. The improved activity is as a result of photoabsorption of visible light by the doped powders causing generation of electrons and holes. The material may be proposed to be suitable for use in photodegradation of toxic organic substances, dyes, and other colorless organic substances. The results of this research work indicate that the effect of annealing temperature on the synthesis of $Bi_{0.65}K_{0.2}Ba_{0.15}FeO_3$ show enhanced photocatalytic activity in the presence of hydrogen peroxide leading to improved performance for MB photodegradation under visible light irradiation.

Abbreviations

K2BFO: Potassium-doped bismuth barium ferrite; MB: Methylene blue; PXRD: Powder X-ray diffraction; SDS: Sodium dodecyl sulfate; SEM: Scanning electron microscopy

Acknowledgements

The authors wish to thank Dr. Abdulkadir Tanimu of the Department of Chemistry King Fahd University of Petroleum and Minerals (KFUPM), Dhahran-Saudi Arabia, for helping with some of the analysis and Ahmadu Bello University Zaria, Nigeria, for proving us with the facilities available to carry out this work.

Authors' contributions

AH and IA designed the experimental approach, carried out the synthesis of the material, and wrote the manuscript. Together, they did the characterization of the perovskite nanoparticles. AH carried out the photocatalytic studies against MB dye pollutants under visible light irradiation. AH generated all the figures and tables in the manuscript and helped to draft the manuscript. All authors read and approved the final manuscript.

Funding

The study was self-sponsored and no funding was received from any agency.

Availability of data and materials

Data sharing is not applicable to this article as no data sets were generated or analyzed during the current study.

Ethics approval and consent to participate

Not applicable

Consent for publication

Not applicable

Competing interests

The authors declare that they have no competing interests.

Received: 18 October 2019 Accepted: 6 January 2020
Published online: 03 March 2020

References

1. Tan YN, Wong CL, Mohamed AR (2011) An overview on the photocatalytic activity of nano-doped-TiO_2 in the degradation of organic pollutants. ISRN Mat. Sci. 2011:18
2. Fujishima, A., Rao, T. N., and Tryk, D. A. (2000). Titanium dioxide photocatalysis. *Journal of Photochemistry and Photobiology C: Photochemistry Reviews, 1*(1), 1–21. https://doi.org/10.1016/S1389-5567(00)00002-2
3. Linsebigler AL, Lu G, Yates JT Jr (1995) Photocatalysis on TiO_2 surfaces: principles, mechanisms, and selected results. Chemical Review. 95(1995):735 https://doi.org/10.1021/cr00035a013
4. Guo C, Wu X, Yan M, Dong Q, Yin S, Sato T, Liu S (2013) The visible-light driven photocatalytic destruction of NO_x using mesoporous TiO_2 spheres synthesized via a "water-controlled release process". *Nanoscale*. 5:8184–8191
5. Zhao J, Yang X (2003) Photocatalytic oxidation for indoor air purification: a literature review. Build. Environ. 38:645–654
6. Lasek J, Yu Y-H, Wu JCS (2013) Removal of NO_x by photocatalytic processes. *Journal of Photochemistry Photobiology*. 14:29–52
7. Ahmed S, Rasul MG, Martens W, Brown R, Hashib MA (2011) Advances in heterogeneous photocatalytic degradation of phenols and dyes in wastewater: a review. *Water Air Soil Pollution*. 215:3–29
8. Rajesh JT, Praveen KS, Ramchandra GK, Raksh VJ (2007) Photocatalytic degradation of dyes and organic contaminants in water using nanocrystalline anatase and rutile TiO_2. Sci. Technol. Adv. Mat. 8:455
9. Kanhere P, Chen Z (2014) A review on visible light active perovskite-based photocatalysts. *Molecules 19*(12):19995–20022 https://doi.org/10.3390/molecules191219995
10. Ohtani, B. (2011). Journal of Photochemistry and Photobiology C : Photochemistry reviews photocatalysis A to Z—what we know and what we do not know in a scientific sense. *"Journal of Photochemistry & Photobiology, C: Photochemistry Reviews," 11*(4), 157–178. https://doi.org/10.1016/j.jphotochemrev.2011.02.001
11. Qu Y, Duan X (2013) Progress, challenge and perspective of heterogeneous photocatalysts. *Journal of Chemical Society Review*. 42:2568–2580
12. Cook TR, Dogutan DK, Reece SY, Surendranath Y, Teets TS, Nocera DG (2010) Solar energy supply and storage for the legacy and nonlegacy worlds. *Journal of Chemical Review*. 110:6474–6502
13. Woodward, P. M. (1997). Octahedral tilting in perovskites. Ll. Structure stabilizing forces. *Acta Crystallographica Section B, 53*(1), 44-66.
14. Yang Y, Yanbin S, Yinshan J (2006) Structure and photocatalytic property of perovskite and perovskite-related compounds. *J. Materials Chemistry and Physics* 96:234–239
15. Bhalla AS, Guo R, Roy R (2000) The perovskite structure–a review of its role in ceramic science and technology. *Journal of Material Resources Innovation*. 4:3–26
16. Nuraje, N. and Su, K. (2013). Perovskite ferroelectric nanomaterials. Nanoscale *Molecules*, 19(14), 5, 8752–8780.https://doi.org/10.1039/C3NR02543H.
17. Jia Q, Iwase A, Kudo A (2014) BiVO4-Ru/SrTiO3: Rh composite Z-scheme photocatalyst for solar water splitting. *Journal of Chemical Science*. 5:1513–1519
18. Sayama K, Mukasa K, Abe R, Abe Y, Arakawa H (2001) Stoichiometric water splitting into H_2 and O_2 using a mixture of two different photocatalysts and an $IO3^-/I^-$ shuttle redox mediator under visible light irradiation. *Chemical Communication*. 23:2416–2417
19. Feng, W., Hong, X., Wang, H., and Tao, J. (2004). Photocatalytic property of perovskite bismuth titanate, *52*, 109–116. https://doi.org/10.1016/j.apcatb.2004.04.002
20. Hu Z, Chen D, Wang S, Zhang N, Qin L, Huang Y (2017) Facile synthesis of Sm doped $BiFeO_3$ nanoparticles for enhanced visible light photocatalytic performance. *Materials Science & Engineering B 220*:1–12 https://doi.org/10.1016/j.mseb.2017.03.005
21. Lam S, Sin J, Mohamed AR (2016) A newly emerging visible light-responsive $BiFeO_3$ perovskite for photocatalytic applications: a mini review. *Materials Research Bulletin*. 90:15–30 https://doi.org/10.1016/j.materresbull.2016.12.052

22. Haruna A, Abdulkadir I, Idris SO (2018) Visible light induced photodegradation of methylene blue in sodium doped bismuth barium ferrite nanoparticle synthesized by sol-gel method. *Avicenna Journal of Environmental Health Engineering*. 5(2):120–126 https://doi.org/10.15171/ajehe.2018.16
23. Wang B, Wang S, Gong L, Zhou Z (2012) Structural, magnetic and photocatalytic properties of Sr 2-doped $BiFeO_3$ nanoparticles based on an ultrasonic irradiation assisted self-combustion method. *Ceramics International 38*(8):6643–6649 https://doi.org/10.1016/j.ceramint.2012.05.051
24. Soltani, T. and Lee, B. K. (2016). Novel and facile synthesis of Ba-doped $BiFeO_3$ nanoparticles and enhancement of their magnetic and photocatalytic activities for complete degradation of benzene in aqueous solution. *Journal of Hazardous Materials* (Vol. 316). Elsevier B.V. https://doi.org/10.1016/j.jhazmat.2016.03.052
25. Haruna, A., Abdulkadir, I. and Idris, S. O. (2019). Synthesis, characterization and photocatalytic properties of $Bi_{0.85-X}M_XBa_{0.15}FeO_3$ (M = Na and K, X = 0, 0.1) perovskite-like nanoparticles using the sol-gel method. Journal of King Saud University –Science, https://doi.org/10.1016/j.jksus.2019.05.005
26. Huang M, Xu C, Wu Z, Huang Y, Lin J, Wu J (2008) Photocatalytic discolorization of methyl orange solution by Pt modified TiO_2 loaded on natural zeolite. *Dyes and Pigments*. 77(2):327–334
27. Bettinelli M, Dallacasa V, Falcomer D (2007) Photocatalytic activity of TiO_2 doped with boron and vanadium. *Journal of Hazardous Materials*. 146(3): 529–534
28. Senthilnathan J, Philip L (2010) Photocatalytic degradation of lindane under UV and visible light using N-doped TiO_2. *Chemical Engineering Journal* 161(1-2):83–92
29. Li J, Cai D, Song J, Jin D, Yu S, Cheng J (2010) Synthesis and photocatalytic property of Ba-doped BiFeO3nanoparticles. *Proceedings of the 2010 IEEE International Symposium on the Applications of Ferroelectrics, ISAF 2010, Co-Located with the 10th European Conference on the Applications of Polar Dielectrics, ECAPD 2010 1*(1):3–6 https://doi.org/10.1109/ISAF.2010.5712271
30. Abdulkadir I, Jonnalagadda SB, Martincigh BS (2016) Synthesis and effect of annealing temperature on the structural, magnetic and photocatalytic properties of $(La_{0.5}Bi_{0.2}Ba_{0.2}Mn_{0.1})FeO_{(3\_d)}$. *Materials Chemistry and Physics 178*:196–203 https://doi.org/10.1016/j.matchemphys.2016.05.007
31. Soltani T, Entezari MH (2014) Solar-Fenton catalytic degradation of phenolic compounds by impure bismuth ferrite nanoparticles synthesized via ultrasound. *Chemical Engineering Journal* 251:207–216 https://doi.org/10.1016/j.cej.2014.04.021
32. Gupta S, Tomar M, Gupta V, James AR, Pal M, Guo R, Bhalla A (2014) *Optimization of excess Bi doping to enhance ferroic orders of spin casted BiFeO3 thin film. Journal of Applied Physics 115(23):234105*. https://doi.org/10.1063/1.4884680
33. Suresh P, Srinath S (2015) *Effect of synthesis route on the multiferroic properties of $BiFeO_3$: a comparative study between solid state and sol–gel methods. Journal of Alloys and Compounds 649:843–850.* https://doi.org/10.1016/j.jallcom.2015.07.152
34. Rashad MM (2012) Effect of synthesis conditions on the preparation of $BiFeO_3$ nanopowders using two different methods. *Journal of Materials Science: Materials in Electronics*. 23(4):882–888
35. Wang X, Lin Y, Zhang ZC, Bian JY (2011) Photocatalytic activities of multiferroic bismuth ferrite nanoparticles prepared by glycol-based sol-gel process. *Journal of Sol-Gel Science and Technology 60*(1):1–5 https://doi.org/10.1007/s10971-011-2542-4
36. Chang DA, Lin P, Tseng TY (1995) Optical properties of ZrTiO4 films grown by radio-frequency magnetron sputtering. Journal of Applied Physics. 77: 4445–4451
37. Soltani T, Entezari MH (2013) Photolysis and photocatalysis of methylene blue by ferrite bismuth nanoparticles under sunlight irradiation. *Journal of Molecular Catalysis A: Chemical*. 377(3):197–203
38. Rahmani A, Rahimzadeh H, Beirami S (2018) Photo-degradation of phenol using TiO_2/CMK-3 photo-catalyst under medium pressure UV lamp. *Avicenna Journal of Environmental Health Engineering*. *5*(1):35–41 https://doi.org/10.15171/ajehe.2018.05

Publisher's Note